J Mater Sci: Mater Electron (2015) 26:4691–4697
DOI 10.1007/s10854-015-2877-7

High temperature optical absorption investigation into the electronic transitions in sol–gel derived C12A7 thin films

Elnaz Feizi · Asim K. Ray

Received: 18 January 2015 / Accepted: 23 February 2015 / Published online: 4 March 2015

Abstract Optical absorption into 6 mm thick sol–gel derived films, annealed at 1300 °C of $12CaO{\cdot}7Al_2O_3$ calcium aluminate binary compound on MgO⟨100⟩ single crystal substrates was studied at temperatures ranging from room temperature to 300 °C. Experimental data were analysed in both Tauc and Urbach regions. The optical band gap decreased from 4.088 eV at 25 °C to 4.051 eV at 300 °C, while Urbach energy increased from 0.191 eV at 25 °C to 0.257 eV at 300 °C. The relationship between the optical band gap and the Urbach energy at different temperatures showed an almost linear relationship from which the theoretical values of 4.156 and 0.065 eV were evaluated for the band gap energy and Urbach energy of a $12CaO{\cdot}7Al_2O_3$ crystal with zero structural disorder at 0 K.

1 Introduction

The complex oxide $12CaO{\cdot}7Al_2O_3$, or C12A7, has been widely known for several years as one of the main constituents of alumina cements. Its unique crystal structure, however, has been only recently understood. The lattice structure of this compound is built up of nano-sized empty cages of $[Ca_{24}Al_{28}O_{64}]^{4+}$ which can randomly incorporate negatively charged species, such as O^{2-}, O^-, O_2^{2-}, F^-, Cl^-, OH^-, H^- and electrons [1, 2], the properties of the compound being dependent upon the type and concentration of these species [3]. For instance, this insulating material can be converted to a semiconductor, conductor or superconductor depending on the type of incorporated anions without a significant change in the structure of the lattice [4, 5]. This complex oxide is, therefore, gaining much attention in numerous chemical, electronic and optoelectronic applications such as ion conductor, electron donor for chemical syntheses and decomposition reactions, electron field emitter, electron injection layers in organic light-emitting devices, oxidizing/reducing agent, ion emitter, and as a transparent conductive oxide in flat panel displays, solar cells and transparent transistors [6–10]. Such a wide range of applications for C12A7 has led to an increasing demand for the fabrication and characterisation of high quality thin films. However, only a limited number of reports are focused on thin film production and characterisation. Two fabrication techniques, which have been previously suggested for the preparation of C12A7 thin films, include pulsed laser deposition [11–14] and sol–gel spin coating method [15, 16]. The former technique is relatively costly and requires a C12A7 target as the starting material for the deposition of the film while obtaining a continuous defect-free thin oxide film with a high critical thickness using sol–gel technique is found to be quite challenging. Therefore, sol–gel method is often chosen for the production of C12A7 powder [17, 18]. The crystallisation of C12A7 consisting of calcium oxide (CaO) and aluminium oxide (Al_2O_3) in a ratio of 12:7 takes place at 1100 °C and values of 348 and 375 kJ/mol have been estimated from the Kissinger's equation for the activation energies of crystallisation of CaO and Al_2O_3 components, respectively [19]. However, it has been recently reported that the addition of ethyl acetoacetate (EAA) to the oxide sol reduces the densification oxide gel significantly leading

E. Feizi · A. K. Ray
Centre for Materials Research, Queen Mary, University of London, Mile End Road, London E1 4NS, UK

A. K. Ray (✉)
Institute of Materials and Manufacturing, Brunel University London, Uxbridge, Middlesex UB8 3PH, UK
e-mail: Asim.Ray@brunel.ac.uk

to the prolonged structural relaxation during heat treatment [20].

Using EAA as a chelating agent with aluminium sec-butoxide (ASB) in the spreading solution, we have successfully deposited high quality 5–6 μm thick C12A7 thin films on magnesium oxide (MgO) single crystal substrates by spin coating method. Vibrational spectroscopic measurements showed the formation of a single-phase C12A7 film when as-deposited film was annealed at 1300 °C and the heat treatment duration had no significant effect on the formation of calcium aluminate phases [21]. The present article reports the optical absorption properties of sol–gel derived C12A7 thin films and the effect of temperature on optical parameters, such as band gap energy, Urbach energy and steepness parameter have been examined in terms of relevant physical models. Extra framework ion species are found to be responsible for the location of absorption edge; the interpretation of the optical absorption behaviour of C12A7 is one of the most beneficial methods in order to have a good understanding of the electronic structure of the material and evaluating the energy band diagram [22].

2 Experimental procedure

Thin films of C12A7 were fabricated using sol–gel technique. A solution was prepared using stoichiometric ratios of aluminium sec-butoxide (ASB) and calcium nitrate tetrahydrate as the main precursors of aluminium oxide and calcium oxide respectively. In order to increase the homogeneity and continuity of the films, a modified solution recipe containing ethyl acetoacetate (EAA) and ASB in the molar ratio of 2:1 and isopropyl alcohol as solvent was developed. Thin films were prepared via spin coating on magnesium oxide (MgO) single crystal substrates and subsequent isothermal annealing at 1300 °C was performed for 2 h under air atmosphere in order to obtain a single-phase crystalline structure. The details of the sample preparation are given in our previous publication [21]. The thickness of the films on MgO substrates were measured by means of a Dektak 150 surface profiler.

The microstructural surface of the films after heat treatment was examined using JEOL JSM-6300 field-emission scanning electron microscope in order to confirm the formation of continuous films with high surface quality. The absorbance of the thin films was measured in a temperature range of 25–300 °C to investigate the effect of temperature on the optical absorption properties of the films. A U-3010 UV–Vis spectrometer provided by Hitachi and equipped with a hot chamber and a Mettler FP 80 central processor was used for this type of measurement. The absorbance spectra of the samples were obtained for temperature intervals of 10 °C in a wavelength range of 200–900 nm. The absorbance of MgO substrate was measured simultaneously and was set as the baseline value.

3 Results and discussion

Figure 1 shows the formation of a completely crystallised microstructure with distinct grain boundaries. This indicates that full transformation of intermediate phases into the most stable thermodynamic phase has occurred via nucleation and growth mechanism. In addition, the surface of the annealed film is continuous and crack-free.

3.1 Room temperature absorption spectrum

The presence of two broad absorption peaks at 4.5 and 5.39 eV in the ultraviolet wavelength region is evident from Fig. 2a displaying the absorbance of C12A7 films as a function of incident photon energies hυ between 1 and 6 eV. The first electronic transition in the range between 3.6 and 4.4 eV is believed to have occurred from the occupied electronic state of extra-framework O^{2-} ions to the cage conduction band while the second transition in the range between 4.6 and 5.6 eV may be attributed to the excitation from the occupied state of O^{2-} to the framework conduction band [23]. The plot of $(\alpha h\upsilon)^2$ against hυ in the first regime above the threshold of absorption edge, shown in Fig. 2b, is linear according to Tauc's law in the form [24]:

$$\alpha(h\upsilon) \propto \frac{(h\upsilon - E_g)^{1/2}}{h\upsilon} \quad (1)$$

where the values of the absorption coefficient α are determined from Fig. 2a using Beer's law. This square root

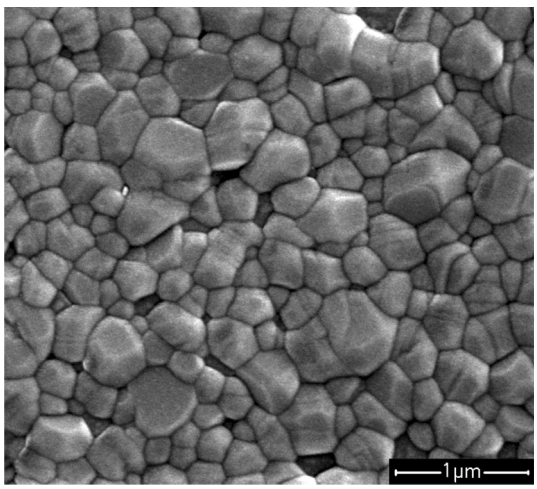

Fig. 1 SEM image of C12A7 thin film heat treated at 1300 °C for 2 h in air atmosphere

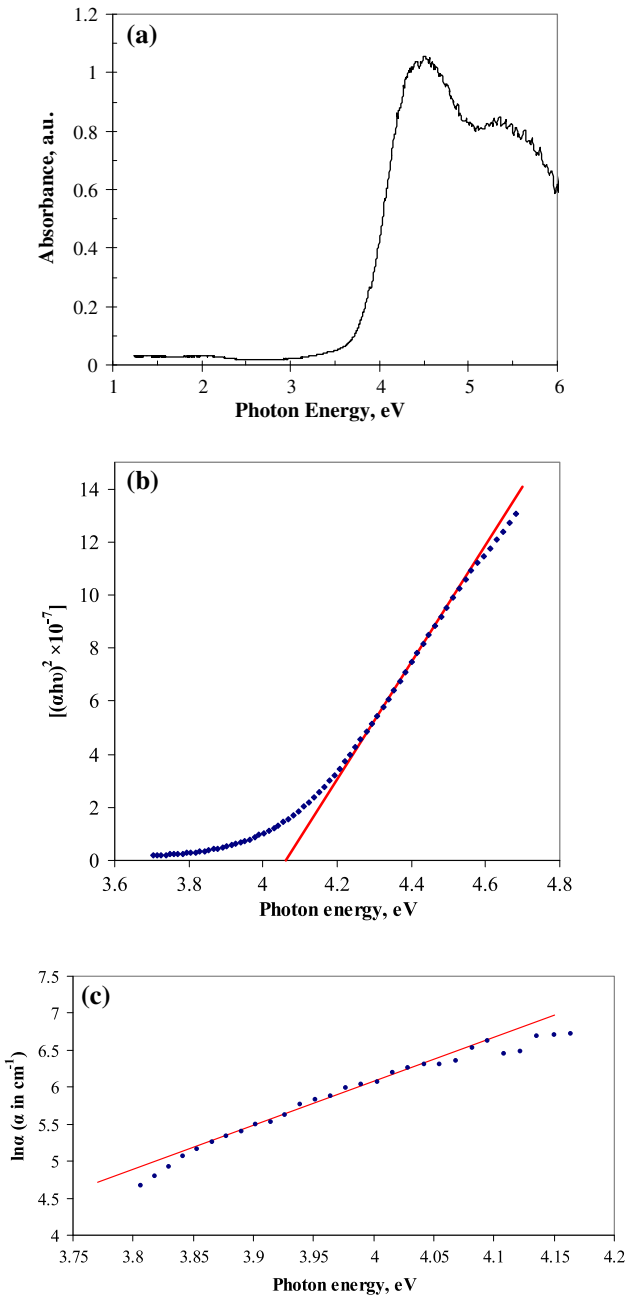

Fig. 2 **a** Room temperature absorbance spectrum of C12A7 thin film, **b** Tauc and **c** Urbach plots

law dependence indicates an allowed direct type of transition. A value of 4.1 eV is determined for the optical band gap E_g from the intercept on the ordinate extrapolated to $h\upsilon = 0$. The absorption edge of C12A7 framework has been reported to be ~6.8 eV corresponding to the fundamental absorption of the material. However, the presence of extra-framework species has a significant effect on the absorption edge. The absorption edge is shifted to lower energy values as a result of transition from an occupied state of the species to the framework conduction band [25]. The transitions from the occupied states to the cage conduction band have much lower densities, and therefore, the effect of these types of transitions on the absorption band shift is negligible. The extra-framework O^{2-} ions have the most significant effect on the absorption edge shift among all types of extra-framework species [26]. Using the Lorentz–Lorenz equation for electronic polarizability in the modified form of $\frac{n^2-1}{n^2+2} = 1 - \sqrt{\frac{E_g}{20}}$ [27], the refractive index for C12A7 film is estimated to be 1.86.

For the tail of absorbance for $h\upsilon < 4.1$ eV the variation of $\ln\alpha$ as a function of $h\upsilon$ in Fig. 2c is found to be linear. Therefore this dependence can be expressed as the Urbach law in an exponential form [28]:

$$\alpha(h\upsilon) = \alpha_o \exp\left(\frac{\sigma(h\upsilon - E_o)}{k_B T}\right) \quad (2)$$

where α_o, σ and E_o are fitting parameters. E_o is the energy of the lowest free exciton state at zero lattice temperature while σ corresponds to the steepness of the absorption edge. T and k_B are the absolute ambient temperature and Boltzmann's constant, respectively. A value of 0.19 eV is obtained for the Urbach energy $E_U = \frac{kT}{\sigma}$ of the C12A7 thin films at room temperature.

3.2 Effect of ambient temperature on optical absorption

The plots of the absorption coefficient within the tail regime as a function of photon energy on logarithm-linear are shown in Fig. 3 for temperatures ranging from 25 to 300 °C. The extrapolations of the plots converge to a single point with the coordinates, giving the values of $E_o = 4.23$ eV and $\alpha_o = 1.4\times10^3$ cm^{-1}.

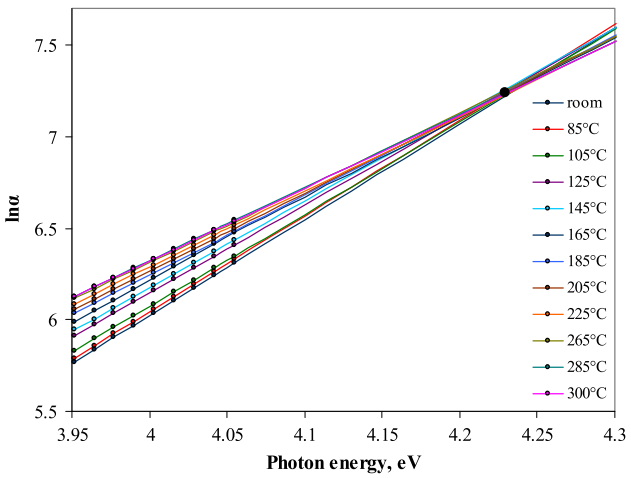

Fig. 3 Semi-logarithmic plots of the absorption coefficient as a function of photon energy in the Urbach region for a temperatures range between 25 and 300 °C

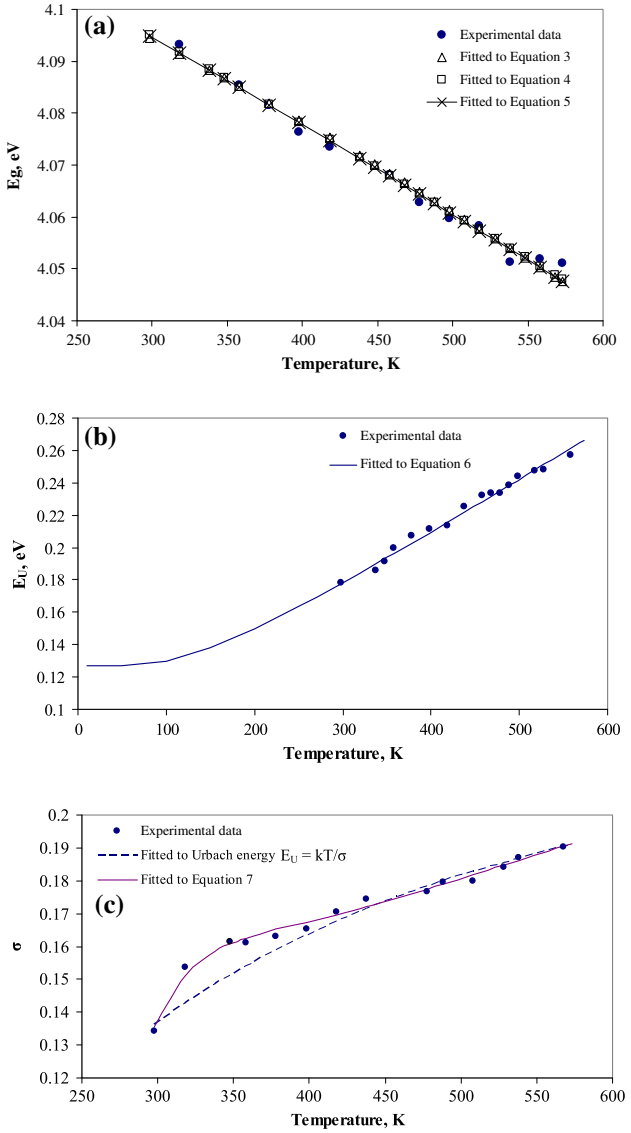

Fig. 4 Temperature dependence of (**a**) band gap energy E_g, **b** Urbach energy E_U and **c** steepness parameter σ

Figure 4 shows the dependence of optical band gap E_g, Urbach energy E_U and steepness of the absorption edge σ on the ambient temperature T. A continual decrease of optical band gap E_g with the increase in temperature was observed while E_U was found to be rising with temperature. In both cases, the variation is nearly linear. Monotonic increase in σ with T, however, was found to nonlinear. The interatomic spacing is expected to increase with the temperature rise because the amplitude of atomic vibrations becomes larger due to greater thermal energy. This increased interspacing distance reduces the potential as seen by electrons yielding a decrease in E_g. The dependence of E_g on T in Fig. 4a may be expressed by the following expression proposed by Varshni [29]:

$$E_g(T) = E_g(0) - \frac{\alpha T^2}{T + \theta_D} \tag{3}$$

where $E_g(0)$ is the energy gap at T = 0 K and θ_D is related to the Debye temperature. The Varshni coefficients $\alpha = 2.3\times10^{-4}$ eV K^{-1} and $\theta_D = 450$ K were determined from the least squares fit to the experimental data. A value of $E_g(0) = 4.12$ eV was also estimated from the same procedure.

Equation (3) works well at moderately high temperatures. However, it predicts the T^2 law dependence of E_g at low temperatures and this is not in keeping with experimental observation of temperature independence of E_g over this regime. The type of behaviour in Fig. 4a is attributed to the change in the relative positions of the valence and conduction bands due to the dilation of the lattice and the electron–phonon interactions being dependent upon temperature [30]. These thermal effects can better be described by an empirical Manoogian-Leclerc equation in the form [31]:

$$E_g(0) - E_g(T) = UT^x + V\theta_D\left(\coth\frac{\theta_D}{T} - 1\right) \tag{4}$$

where $E_g(0)$ is the energy gap at T = 0 K and the parameters x, U and V are constants and independent of temperature. The Debye temperature θ_D corresponds to the mean frequency of the entire phonon spectrum. Values of 4.13 eV, 1.05, 2.7×10^{-5} eV $K^{-1.05}$ and 7.1×10^{-5} eV K^{-1} for the parameters $E_g(0)$, x, U and V are estimated from the best numerical fitting of Eq. (4) to experimental data by using the least squares of standard deviation technique. The inclusion of the Bose–Einstein oscillators in Eq. (4) has also been suggested as the first order approximation to describe the lattice vibration [32].

$$E_g(T) = E_g(0) - \frac{2a_B}{\exp\left(\frac{\Theta_E}{T}\right) - 1} \tag{5}$$

where a_B is a measure of the electron–phonon interaction coupling. Θ_E, which is known as Einstein temperature, is the average temperature of the interacting phonons representing the Einstein model for solids. The least square fit of Eq. (5) to experimental data produced the values of $E_g(0) = 4.12$ eV and $a_B = 3.5 \times 10^{-2}$ eV giving good agreement between the model and experiment as shown in Fig. 4a.

As shown in Fig. 4b, the Urbach energy E_U is a linearly increasing function of temperature. Both the structural disorder of the material and phonon energy define the Urbach tail. The value of Urbach energy may thus be dependent upon different chemical methods of preparation of the material [33]. The thermal and structural disorders are additive and the Urbach energy can be expressed as the

sum of two terms in the following form suggested by Cody et al. [34]:

$$E_U(X,T) = \frac{k_B\Theta_E}{\sigma_o}\left[\frac{X+1}{2} + \frac{1}{\exp(\Theta_E/T)-1}\right] \quad (6)$$

where k_B is the Boltzmann constant, Θ_E is the Einstein Temperature, σ_o is an Urbach parameter depending on the ionicity of the material and $X = \frac{\langle U_x\rangle}{\langle U_0\rangle}$ is a measure of the degree of the structural disorder of the material normalised to zero-point uncertainty in the atomic position $\langle U_0\rangle$. $\langle U_x\rangle$ is the structural and topological disorder to the mean square deviation of atomic positions from perfectly ordered configurations. These disorders may be caused by intrinsic defects such as vacancies or dislocation, or extrinsic factors such as radiation and/or doping.

The Debye temperature, θ_D, was estimated to be 471.5 K for C12A7 film using the relation $\theta_D = \left(\frac{6}{\pi}\right)^{\frac{1}{3}}\Theta_E$. The fitted line of the formula (6) is best described with the phonon energy of 32 meV which is equivalent to the Raman band of 258 cm^{-1} [35]. This Raman band is associated with the vibration modes of the framework Ca^{2+} ions and has been reported to be responsible for the occurrence of Urbach tail in C12A7 [36].

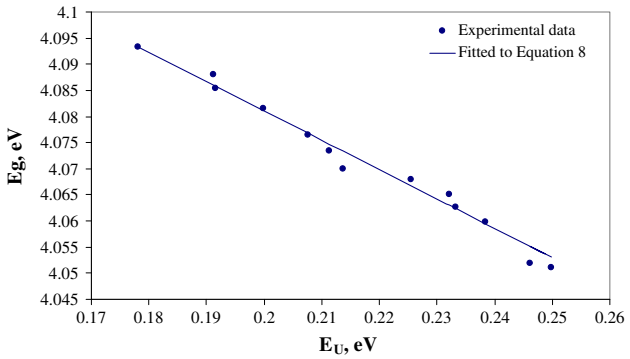

Fig. 5 Relationship between the band gap energy (E_g) and Urbach energy (E_U) obtained at different temperatures

The temperature dependence of the steepness parameter can also be expressed by the following relation [37]:

$$\sigma = \frac{2\sigma_o k_B T}{h\upsilon_o}\tanh\left(\frac{h\upsilon_o}{2k_B T}\right) \quad (7)$$

where $h\upsilon_o$ is the phonon energy interacting with the optical transitions. The value of constant σ_o indicates the strength of the exciton-phonon interaction $g = \frac{2}{3}\sigma_o^{-1}$. Using Taylor's series approximation, Eq. (7) is fitted to experimental data in Fig. 4c. The values of the slopes of the straight lines in Fig. 3 on the semi-logarithmic absorption coefficient scales were used to obtain these data. The fitting parameters were found to be $\sigma = 0.23$, $h\upsilon = 0.079$ eV and $g = 2.9$. The value of $g > 1$ predicts the existence of self-trapped excitons in the exciton-phonon coupling [38].

If $E_g(X, T)$ and $E_U(X, T)$ are the band gap energy and the Urbach energy of the material with finite degree of structural disorder at a fixed temperature, the relation between them may be written in an empirical form [39]:

$$E_g(X,T) = E_g(0,0) - \langle U^2\rangle_o D\left[\frac{E_U(X,T)}{E_U(0,0)} - 1\right] \quad (8)$$

The linear relationship between the band gap energy and the Urbach energy in Fig. 5 for a temperature range of 25–300 °C is in keeping with the law in Eq. (8). Values of 4.2 eV and 65.5 meV are obtained for the band gap energy E_g (0, 0) and the Urbach energy E_U(0, 0) of a defect-free crystal at 0 K, respectively from the least squares fitting of Eq. (8) to experimental data. D is the second-order deformation potential that determines the effect of temperature on the band gap energy and the product $\langle U^2\rangle_o D$ is found to be 36.5 meV.

4 Conclusions

Values of parameters of the models which have been used to interpret experimental data have been summarised in Table 1. An optimised sol–gel process was used in order to

Table 1 Values of parameters of the model obtained from the least squares fitting procedure

Parameter	Fitted value	Equation no.	Parameter	Fitted value	Equation no.
E_g (0) (eV)	4.122	(3)	$h\upsilon_o$ (meV)	79	(7)
	4.127	(4)	σ_o	0.25	(6)
	4.122	(5)		0.23	(7)
U (ev $K^{-1.05}$)	2.7×10^{-5}	(4)	X	0.94	(6)
x	1.05	(4)	Θ_E (K)	380	(6)
V (eV K^{-1})	7.1×10^{-5}	(4)	g	2.9	(7)
α (eV K^{-1})	2.3×10^{-4}	(3	E_g (0,0) (eV)	4.2	(8)
Θ_D (K)	450	(3)	E_U (0,0) (meV)	65.5	(8)
	471.5	(6)	$\langle U^2\rangle_o D$ (meV)	36.5	(8)
a_B (meV)	35	(5)			

produce homogeneous thin films of $12CaO{\cdot}7Al_2O_3$ complex oxide with high critical thickness ($\sim$5–6 mm). The agreement between values of experimentally observed bandgap and its calculated defect-free sample is satisfactorily close. The optical characterisation of C12A7 films showed a reduction in the band gap energy E_g from 4.088 eV at room temperature to 4.051 eV at 300 °C, while the Urbach energy E_U increased from 0.191 eV at 25 °C to 0.257 eV at 300 °C. A linear relationship was observed between the optical band gap energy and the Urbach energy at different temperatures.

Acknowledgments Thanks are due to Professor M.J. Cook and Dr I. Fernades of the School of Chemistry, University of East Anglia, for their permission of use of high temperature optical absorption facilities. The first author (E.F.) is grateful to L.P. Displays Ltd, Blackburn, U.K. for partial funding of the studentship at Queen Mary, University of London.

References

1. S.W. Kim, Y. Toda, K. Hayashi, M. Hirano, H. Hosono, Synthesis of a room temperature stable $12CaO{\cdot}7Al_2O_3$ electride from the melt and its application as an electron field emitter. Chem. Mater. **18**, 1938–1944 (2006). doi:10.1021/cm052367e
2. H. Yanagi, T. Kuroda, K. Kim, Y. Toda, T. Kamiya, H. Hosono, Electron injection barriers between air–stable electride with low work function, C12A7:e^-, and pentacene, C60 and copper phthalocyanine. J. Mater. Chem. **22**, 4278–4281 (2012). doi:10.1039/C2JM14966D
3. P.V. Sushko, in *Tuning Optical Properties of Complex Oxides: Examples of* $12CaO{\cdot}7Al_2O_3$ *Mayenite and* $LaCrO_3$ *Perovskite*; Oxide-Based Materials and Devices III Book Series: Proceedings of SPIE, vol. **8263**, 826310, 2012. doi:10.1117/12.912844
4. S. Matsuishi, H. Muramatsu, H. Hosono, Photochemistry of nanocage $Ca_{12}Al_{14-x}Si_xO_{32}Cl_{2+x}$ (x = 0.0 and 3.4) crystals. Chem. Lett. **43**, 1371–1373 (2014). doi:10.1246/cl.140423
5. S.W. Kim, S. Matsuishi, M. Miyakawa, K. Hayashi, M. Hirano, H. Hosono, Fabrication of room temperature-stable 12CaO·7Al(2)O(3) electride: a review. J. Mater. Sci. Mater. Electron. **18**, S5–S14 (2007)
6. N. Kuganathan, H. Hosono, A.L. Shluger, P.V. Sushko, Enhanced N_2 dissociation on Ru-loaded inorganic electride. J. Am. Chem. Soc. **136**, 2216–2219 (2014). doi:10.1021/ja410925g
7. L. Palacios, A.G. De La Torre, S. Bruque, J.L. Garcia-Munoz, S. Garcıa-Granda, D. Sheptyakov, M.A.G. Aranda, Crystal structures and in situ formation study of mayenite electrides. Inorg. Chem. **46**, 4167–4176 (2007). doi:10.1021/ic0700497
8. Q. Chen, K. Yoshida, H. Yamamoto, M. Uchida, M. Sadakata, Investigation on the application of C12A7 in flue gas desulfurization at low-moderate temperature. Energy Fuels **21**, 3264–3269 (2007). doi:10.1021/ef700268v
9. F. Hayashi, M. Kitano, T. Yokoyama, M. Hara, H. Hosono, Surface treatment for conductive $12CaO{\cdot}7Al_2O_3$ electride powder by rapid thermal annealing processing and its application to ammonia synthesis. ChemCatChem **6**, 1317–1323 (2014). doi:10.1002/cctc.201301061
10. M. Zahedi, A.K. Ray, D.S. Barratt, Novel binary calcia–alumina systems for device applications. Sci. Adv. Mater. **1**(2), 107–120 (2009)
11. M. Miyakawa, Fabrication of high-density electron-doped $12CaO{\cdot}7Al_2O_3$ thin films by physical and chemical processes. J. Ceram. Soc. Jpn. **117**(3), 395–401 (2009). doi:10.2109/jcersj2.117.395
12. M. Miyakawa, M. Hirano, T. Kamiya, H. Hosono, High electron doping to a wide band gap semiconductor $12CaO{\cdot}7Al_2O_3$ thin film. Appl. Phys. Lett. **90**, 182105 (2007). doi:10.1063/1.2735280
13. H. Yanagi, K. Kim, I. Koizumi, M. Kikuchi, H. Hiramatsu, M. Miyakawa, T. Kamiya, M. Hirano, H. Hosono, Low threshold voltage and carrier injection properties of inverted organic light-emitting diodes with $[Ca_{24}Al_{28}O_{64}]^{4+}(4e^-)$ cathode and $Cu_{2-x}Se$ anode. J. Phys. Chem. C **113**, 18379–18384 (2009). doi:10.1021/jp906386q
14. H. Hosono, S.W. Kim, M. Miyakawa, S. Matsuishi, T. Kamiya, Thin film and bulk fabrication of room-temperature-stable electride C12A7:e^- utilizing reduced amorphous $12CaO{\cdot}7Al_2O_3$ (C12A7). J. Non-Cryst. Solids **354**, 2772–2776 (2008). doi:10.1016/j.jnoncrysol.2007.09.090
15. M. Zahedi, A.K. Ray, D.S. Barratt, Preparation and crystallization of sol–gel C12A7 thin films. J. Phys. D Appl. Phys. **41**, 035404 (2008). doi:10.1088/0022-3727/41/3/035404
16. P.M. Chavhan, A. Sharma, R.K. Sharma, G. Singh, N.K. Kaushik, Dip coated $12CaO{\cdot}7Al_2O_3$ thin films through sol–gel process using metal alkoxide. Thin Solid Films **519**(1), 18–23 (2010). doi:10.1016/j.tsf.2010.07.014
17. K. Ozawa, N. Sakamoto, N. Wakiya, H. Suzuki, Fabrication of $12CaO{\cdot}7Al_2O_3$ powders with high specific surface area by sol–gel and ball-milling method. J. Ceram. Soc. Jpn. **119**(6), 460–463 (2011). doi:10.2109/jcersj2.119.460
18. L. Gong, Z. Lin, S. Ning, J. Sun, J. Shen, Y. Torimoto, Q. Li, Synthesis and characteristics of the C12A7-O^- nanoparticles by citric acid sol–gel combustion method. Mater. Lett. **64**, 1322–1324 (2010). doi:10.1016/j.matlet.2010.03.023
19. M. Zahedi, N. Roohpour, A.K. Ray, Kinetic study of crystallisation of sol–gel derived calcia–alumina binary compounds. J. Alloys Compd. **582**, 277–282 (2014)
20. C. Jing, X. Zhao, Y. Zhang, Sol–gel fabrication of compact, crack-free alumina film. Mater. Res. Bull. **42**, 600–608 (2007). doi:10.1016/j.materresbull.2006.08.005
21. E. Feizi, J.J. Ojeda, A.K. Ray, Vibrational spectroscopic studies on crystallisation of sol–gel derived thin films of calcia–alumina binary compound. J. Mater. Sci. Mater. Electron. **25**, 2261–2266 (2014). doi:10.1007/s10854-014-1869-3
22. K. Hayashi, P.V. Sushko, Ramo D. Munoz, A.L. Shluger, S. Watauchi, I. Tanaka, S. Matsuishi, M. Hirano, H. Hosono, Nanoporous crystal $12CaO{\cdot}7Al_2O_3$: a playground for studies of ultraviolet optical absorption of negative ions. J. Phys. Chem. B **111**, 1946–1956 (2007). doi:10.1021/jp065793b
23. Y. Toda, M. Miyakawa, K. Hayashi, T. Kamiya, M. Hirano, H. Hosono, Thin film fabrication of nano-porous $12CaO{\cdot}7Al_2O_3$ crystal and its conversion into transparent conductive films by light illumination. Thin Solid Films **445**, 309–312 (2003). doi:10.1016/S0040-6090(03)01170-2
24. J. Tauc, in *The Optical Properties of Solids*, ed. by G. Harbeke (Academic Press Inc, New York, 1966)
25. M. Zahedi, A.K. Ray, Optical absorption in solution processed thin films of calcia–alumina binary compounds. J. Sol-Gel. Sci. Technol. **55**(3), 317–321 (2010)
26. P.V. Sushko, Ramo D. Munoz, A.L. Shluger, Electronic structure and spectroscopic properties of interstitial anions in the nanoporous complex oxide $12CaO{\cdot}7Al_2O_3$. Phys. Status Solidi A **204**(3), 663–669 (2007). doi:10.1002/pssa.200673845

27. S. Paul, P.G. Harris, C. Pal, A.K. Sharma, A.K. Ray, Low cost zinc oxide for memristors with high on–off ratios. Mater. Lett. **130**, 40–42 (2007)
28. J.D. Dow, D. Redfield, Toward a unified theory of Urbach's rule and exponential absorption edges. Phys. Rev. B **5**(2), 594–610 (1972). doi:10.1103/PhysRevB.5.594
29. Y.P. Varshni, Temperature dependence of the energy gap in semiconductors. Physica **34**, 149–154 (1967). doi:10.1016/0031-8914(67)90062-6
30. X.R. Li, M.J. Han, X.L. Zhang, C. Shan, Z.G. Hu, Z.Q. Zhu, J.H. Chu, Temperature-dependent band gap, interband transitions, and exciton formation in transparent p-type delafossite $CuCr_{1-x}Mg_xO_2$ films. Phys. Rev. B **90**(3), 035308 (2014)
31. A. Manoogian, J.C. Woolley, Temperature dependence of the energy gap in semiconductors. Can. J. Phys. **62**(3), 285–287 (1984)
32. J. Bhosale, A.K. Ramdas, A. Burger, A. Munoz, A.H. Romero, M. Cardona, R. Lauck, R.K. Kremer, Temperature dependence of band gaps in semiconductors: electron–phonon interaction. Phys. Rev. B **86**(19), 195208 (2012)
33. A.E. Rakhshani, Study of Urbach tail, bandgap energy and grain-boundary characteristics in CdS by modulated photocurrent spectroscopy. J. Phys. Condens. Matter **12**, 4391–4400 (2000). doi:10.1088/0953-8984/12/19/309
34. G.D. Cody, T. Tiedje, B. Abeles, B. Brooks, Y. Goldstein, Disorder and the optical-absorption edge of hydrogenated amorphous silicon. Phys. Rev. Lett. **47**, 1480–1483 (1981). doi:10.1051/jphyscol:1981463
35. K. Kajihara, S. Matsuishi, K. Hayashi, M. Hirano, H. Hosono, Vibrational dynamics and oxygen diffusion in a nanoporous oxide ion conductor $12CaO{\cdot}7Al_2O_3$ studied by ^{18}O labeling and micro-raman spectroscopy. J. Phys. Chem. C **111**(40), 14855–14861 (2007)
36. S. Watauchi, I. Tanaka, K. Hayashi, M. Hirano, H. Hosono, Crystal growth of $Ca_{12}Al_{14}O_{33}$ by the floating zone method. J. Cryst. Growth **237–239**, 801–805 (2002). doi:10.1016/s0022-0248(01)02038-3
37. L.H. Bai, C.C. Xu, P.G. Schunemann, K. Nagashio, R.S. Feigelson, N.C. Giles, Urbach rule used to explain the variation of the absorption edge in $CdGeAs_2$ crystals. J. Phys. Condes. Matter **17**(3), 549–558 (2005)
38. E. Vella, F. Messina, M. Cannas, R. Boscaino, Unraveling exciton dynamics in amorphous silicon dioxide: interpretation of the optical features from 8 to 11 eV. Phys. Rev. B **83**(17), 174201 (2011)
39. K.L. Narayanan, K.P. Vijaykumar, K.G.M. Nair, N.S. Thampi, Effect of irradiation-induced disorder on the optical absorption spectra of CdS thin films. Phys. B **240**(1), 8–12 (1997). doi:10.1016/S0921-4526(97)00428-6